Journal of Neuroscience Methods 179 (2009) 101–110

Contents lists available at ScienceDirect

Journal of Neuroscience Methods

journal homepage: www.elsevier.com/locate/jneumeth

Deconvolution analysis of target evoked potentials

Cliff C. Kerr[a,b,*], Christopher J. Rennie[a,b,c], Peter A. Robinson[a,b,d]

[a] School of Physics, University of Sydney, New South Wales 2006, Australia
[b] Brain Dynamics Center, Westmead Hospital, Westmead, New South Wales 2145, Australia
[c] Department of Medical Physics, Westmead Hospital, Westmead, New South Wales 2145, Australia
[d] Faculty of Medicine, University of Sydney, New South Wales 2006, Australia

ARTICLE INFO

Article history:
Received 1 September 2008
Received in revised form
27 November 2008
Accepted 6 January 2009

Keywords:
Wiener deconvolution
Target analysis
Auditory oddball
Evoked response potential
N1
N2

ABSTRACT

This paper demonstrates a method for analyzing target evoked potentials in an auditory oddball task, using Wiener deconvolution to separate the brain's task-dependent properties from its task-invariant response. It is shown that a target response can be deconvolved, and the result contains two delta-like peaks separated by approximately 100 ms, implying that targets resemble a superposition of two standard responses. The latencies and areas of these delta-like peaks give quantitative measures of the evoked potential, providing a method of analysis that is simpler and more physiologically meaningful than peak scoring. This deconvolution method is applied to both synthetic and experimental evoked potential data, and is demonstrated to be applicable even when normal evoked potential features are not clearly visible.

1. Introduction

Auditory oddball evoked potentials (EPs) are used for a large number of clinical and research purposes, despite the fact that the mechanisms of their generation are still largely unknown. Furthermore, most research has focused on the target P3 component, shown in Fig. 1, and comparatively little work has been done on other target features or on standard responses. Our aim is to present a method for the unified analysis and quantification of the target response that separates it into a task-invariant response (which is common to both targets and standards) and a task-dependent response (which differs between targets and standards).

Clinical EPs are commonly analyzed using peak scoring, which consists of listing the latency and amplitude of a small number of predetermined extremums, shown in Fig. 1A; all other information contained in the EP time series is discarded. Additionally, if the processes that generate different EP components overlap in time, then a change in either amplitude or latency of an underlying process will affect *both* amplitude and latency of the EP components, leading to ambiguity in the physiological interpretation of peak scores.

While numerous studies have applied deconvolution techniques to evoked potentials, to our knowledge, there has been no previous investigation of the use of deconvolution to determine the relationship between target and standard responses. Instead, previous studies have examined the spatial deconvolution of EP and fMRI data (Nunez, 1987; Glover, 1999), Wiener filtering as an alternative to ensemble averaging for extracting EPs from the EEG (Ungan and Başar, 1976; de Weerd, 1981; Wastell, 1981), and the deconvolution of temporally overlapping EPs, using either time-domain or frequency-domain methods. Temporally overlapping EPs are produced when the single-trial EP ("source EP") is convolved with a known stimulus sequence. Time-domain deconvolution methods rely on iteration (Woldorff, 1993) or inversion of the stimulus sequence matrix (Gutschalk et al., 1999; Delgado and Özdamar, 2004) to determine the source EP from the experimental data. Frequency-domain methods (e.g., Hansen, 1983; Jewett et al., 2004) can reproduce the results of time-domain methods (Zhang, 1998; Özdamar and Bohórquez, 2006), and increase the ease of noise filtering, including by Wiener filtering (Wang et al., 2006). However, these time- and frequency-domain methods all require knowledge of the stimulus sequence, and hence the convolution is between a known function (the stimulus sequence) and an unknown function (the source EP). In contrast, time series in seismology are typically convolutions of an unknown source function and the unknown impulse response of the transmission path, and are thus more analogous to the deconvolution problem discussed here. Several deconvolution methods have been successfully applied to seismic data, including Wiener deconvolution (Lines and Ulrych, 2006), homomorphic deconvolution (Ulrych, 1971), and the projected Landweber method (Bertero et al., 1997).

* Corresponding author at: Physics Annex, A29, School of Physics, University of Sydney, NSW 2006, Australia. Tel.: +61 2 9036 7960; fax: +61 2 9351 7726.
E-mail address: ckerr@physics.usyd.edu.au (C.C. Kerr).

0165-0270/$ – see front matter © 2008 Elsevier B.V. All rights reserved.
doi:10.1016/j.jneumeth.2009.01.003

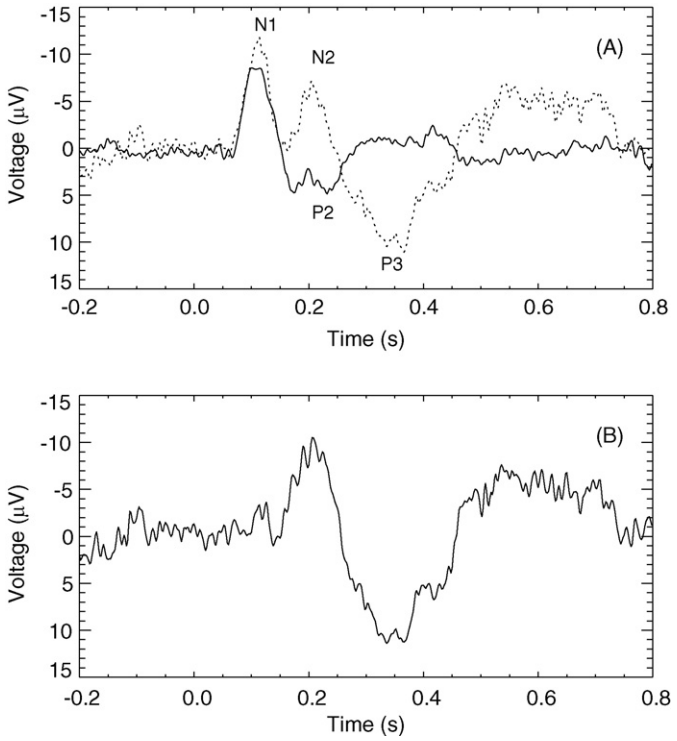

Fig. 1. Evoked potentials from a single subject in an auditory oddball task, recorded from the Cz electrode. (A) Standard (solid) and target (dotted) EPs. (B) The difference signal (or "difference wave"), which resembles a time-shifted standard response.

In EP research, combined analysis of target (or deviant) and standard (or background) responses is typically achieved by simply subtracting the standard response from the target response, resulting in a difference signal (called the "difference wave", although this terminology does not conform to the standard definition of "wave" used in physics). This procedure is motivated by the assumption that certain features of the response are invariant between standards and targets, and thus that targets can be understood more clearly if these shared features are removed. Although difference signals are used in the oddball paradigm (e.g., Pritchard, 1981), the most widely used difference signal is the mismatch negativity, defined as the difference between the responses to deviant and standard tones when no task is required (Näätänen, 1995).

Notably, the difference signal itself is often similar to a time-shifted standard response, as shown in Fig. 1 (e.g., Alho, 1995). This suggests the possibility that the target response is the superposition of two standard responses, one of which is offset by approximately 100 ms. Indeed, a target-like response can be generated by superimposing two standard responses of similar amplitudes and a latency difference of about 70–110 ms, as shown in Fig. 2. While superposition may explain many features of the target response, it is unlikely to completely explain the posterior P3b component (also called P300), which differs from earlier components in its scalp distribution, time course, and dependence on experimental variables (Donchin et al., 1978; Polich, 2007).

One possible physiological explanation of superposition is the sequential activation (or phase synchronization) of one or more anatomically and dynamically similar cortical networks by the thalamus. In this hypothesis, the first activation or synchronization (N1 and P2) results from thalamocortical projection of a stimulus signal, while the second (N2 and P3a) results from corticocortical projection via the thalamus. This hypothesis explains why the delay between N1 and N2 is similar to the estimated thalamocortical loop delay (Rowe et al., 2004), and is consistent with the role of thalamocortical loops as generators of both EPs and ongoing EEG activity (Steriade et al., 1990; Rennie et al., 2002; Kerr et al., 2008). This possibility is considered further in Section 2.3.

Like the difference signal, deconvolution aims to remove the invariant features between targets and standards. However, deconvolution allows these features to be removed without making the assumption that the target consists of an independent signal superimposed on a standard response. This has two advantages: first, it is applicable to targets that appear to contain an amplitude-scaled or time-shifted standard response; second, it is applicable to targets that appear to contain more than one standard response, as suggested by Figs. 1 and 2.

The remainder of this paper is organized as follows. Section 2 describes the general theory of deconvolution, including a specific implementation of Wiener deconvolution, and the experimental data used to demonstrate the method. Section 3 presents the results of the deconvolution of synthetic and experimental data, showing considerable similarity between the deconvolutions of noisy synthetic data and experimental data. Section 4 summarizes the results and describes their possible links to physiology.

2. Theory and methods

2.1. Data and preprocessing

This section describes the synthetic and experimental data used to illustrate the deconvolution method; however, we emphasize that our method does not rely on the details of data acquisition presented in this section.

2.1.1. Synthetic data

A noiseless synthetic standard EP was created by superimposing two Gaussians, one with latency $L = 100$ ms, standard deviation $\sigma = 25$ ms, and amplitude $A = -1.0\,\mu$V, and one with $L = 300$ ms, $\sigma = 75$ ms, $A = 0.5\,\mu$V. A noiseless synthetic target was then generated by superimposing two synthetic standards, the second with a time offset of 100 ms. The resultant time series are shown in Fig. 5A.

Noisy synthetic data were generated by adding brown noise to the data with the form

$$|N(\omega)|^2 = \frac{a}{1+\omega^2/b^2}, \tag{1}$$

where $|N(\omega)|^2$ is the noise power spectrum, ω is angular frequency, a is a scale factor, and $b = 62.8\,\mathrm{s}^{-1} = 10$ Hz modulates the shape of the spectrum. The scale factor was chosen such that the noisy synthetic EPs had a signal-to-noise ratio (SNR) of approximately 2. The resulting noise had amplitude and spectral characteristics comparable to noise in experimental data, as shown in Fig. 5C.

2.1.2. Experimental data

Experimental auditory oddball data were obtained from 43 male subjects (aged 20–30 years; mean 25) via the Brain Resource International Database (Gordon et al., 2005). Recordings were made at 500 Hz from 26 sites of the International 10-10 system using an electrode cap, following previously published methods for acquisition and artifact removal (Rowe et al., 2004; Gordon et al., 2005).

Subjects were presented with a series of standard and target tones (500 and 1000 Hz, respectively), at 75 dB SPL and lasting for 50 ms, with a constant interstimulus interval of 1 s. Subjects were instructed to ignore standard tones, but to respond to target tones with a button press. There were 280 standard and 60 target tones presented in pseudorandom order, with the only constraint being that two targets could not appear consecutively. EP data were extracted from EEG recordings by averaging over a window from –200 ms to 800 ms relative to stimulus onset; target and standard responses were averaged separately.

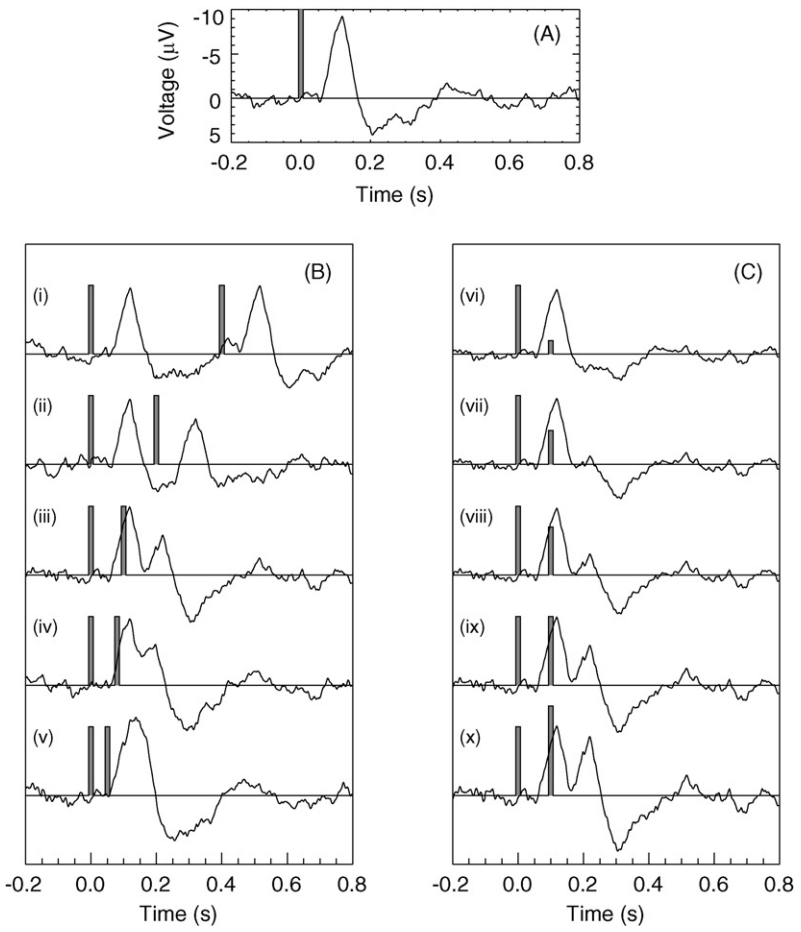

Fig. 2. Generation of a target-like response by superimposing two standard EPs. (A) A standard EP from a single subject was recorded using the Cz electrode (black line). Assuming this standard response is caused by an impulse-like event at $t = 0$ (gray bar), a target-like response can be synthesized using two impulses (columns B and C), which corresponds to the superposition of two amplitude-scaled copies of the standard EP. (B) The effect of different latencies of the second impulse on the synthetic "target". (C) The effect of different amplitudes of the second impulse. Note that subplots (iii), (iv), and (viii)–(x) resemble typical target EPs.

Scoring of the amplitude and latency of each target and standard EP component was performed by Brain Resource Ltd. (Ultimo, NSW, Australia) using an automated system (Haig et al., 1995), with the criteria that N1 was scored between 80 and 140 ms, P2 was scored between 150 and 200 ms, N2 was scored between 205 and 290 ms, and P3 was evident between 280 and 550 ms and not due to EOG contamination (as seen in the EOG channel). Amplitudes were measured relative to a pre-stimulus (200 ms duration) baseline. If automated EP scoring was incorrect (10% of data), a manual scoring of components was undertaken.

Since discontinuities between the initial and final points of the EP time series can cause artifacts when the signal is Fourier transformed, a sigmoidal window function W was applied to the initial and final 200 ms of each time series:

$$W(t) = (1 + e^{(\tau_1 - t)/\sigma})^{-1} - (1 + e^{(\tau_2 - t)/\sigma})^{-1}, \quad (2)$$

where t is the time, $\tau_1 = -100$ ms and $\tau_2 = 700$ ms (relative to stimulus onset) define the midpoints of the sigmoids, and $\sigma = 15$ ms defines their width.

2.2. Deconvolution

Since standard and target stimuli have both similarities (e.g., modality, amplitude, duration, etc.) and dissimilarities (e.g., pitch, task relevance, attention, etc.), the responses to these stimuli would also be expected to have similarities and dissimilarities, as is the case (e.g., N1 and N2, respectively). Additionally, some subcomponents of the nervous system are used to process both types of response (e.g., the cochlea), while others are unique to a single type (e.g., the motor cortex). Thus, the responses to incoming stimuli involve numerous task-invariant and task-dependent subcomponents.

EPs are almost certainly the result of a complex network of interactions between these different subcomponents, and approximations are necessary to make the problem tractable. Specifically, we make the assumption that groups of task-invariant and task-dependent subcomponents are linked serially, allowing these subcomponents (and the stimulus) to be combined into just two functions: a task-invariant function and a task-dependent function. This precludes complex interactions between the two types of subcomponent, but does allow both anatomical separation and complex interactions between subcomponents of a single type. Assuming linearity, the EP time series are produced by convolving these functions:

$$R_S(t) = D_S(t) \otimes I(t) + N_S(t), \quad (3)$$

$$R_T(t) = D_T(t) \otimes I(t) + N_T(t), \quad (4)$$

where $\otimes$ represents convolution; R_S and R_T are the standard and target responses, respectively; D_S and D_T are task-dependent functions for standards and targets, respectively; I is the task-invariant function; and N_S and N_T are noise in the target and standard, respectively. In addition to instrumental noise, the noise terms $N_{S,T}$ include contamination from ongoing EEG activity, as well as any part of the EP response that does not result from the process of

convolution (i.e., the extent to which the assumptions of linearity and serially linked components are invalid).

Despite the fact that Eqs. (3) and (4) are explicitly linear, they are valid regardless of whether EPs are the result of evoked activity or phase synchronization, as long as the resultant signals summate linearly. The calculation of the difference signal also requires this assumption of linearity; however, in contrast to deconvolution, it relies on the assumption that the task-invariant and task-dependent components are activated in parallel, implying an addition between I and $D_{S,T}$ instead of a convolution. No other (simple) assumptions are anatomically possible.

To separate the task-invariant function I from the task-dependent functions D_S and D_T, we first Fourier transform Eqs. (3) and (4), obtaining

$$\tilde{R}_S(\omega) = \mathcal{F}[R_S(t)] = \tilde{D}_S(\omega)\tilde{I}(\omega) + \tilde{N}_S(\omega), \tag{5}$$

$$\tilde{R}_T(\omega) = \mathcal{F}[R_T(t)] = \tilde{D}_T(\omega)\tilde{I}(\omega) + \tilde{N}_T(\omega), \tag{6}$$

where $\mathcal{F}$ denotes a Fourier transform, and tildes denote frequency-domain functions.

If any one of $\tilde{D}_S$, $\tilde{D}_T$, or $\tilde{I}$ can be accurately estimated, the other two functions can be obtained from Eqs. (5) and (6), assuming negligible (or known) noise. However, since none of these functions can be directly obtained from the data, we instead take the ratio of Eqs. (6) and (5). This gives

$$\tilde{D}_C = \frac{\tilde{D}_T}{\tilde{D}_S}\left(1 - \frac{\tilde{N}_S}{\tilde{R}_S}\right) + \frac{\tilde{N}_T}{\tilde{R}_S}, \tag{7}$$

where $\tilde{D}_C$ represents the change in the brain's task-dependent properties between target and standard responses. In the absence of noise ($\tilde{N}_S = \tilde{N}_T = 0$), Eq. (7) simplifies to

$$\tilde{D}_C = \frac{\tilde{D}_T}{\tilde{D}_S}. \tag{8}$$

Finally, an inverse Fourier transform completes the deconvolution:

$$D_C(t) = \mathcal{F}^{-1}[\tilde{D}_C(\omega)]. \tag{9}$$

All differences between the target and standard responses are contained in the deconvolution D_C. Since D_C is produced by an inverse Fourier transform, it is a periodic function, with a period equal to the length of the input data. The time window chosen to represent D_C is arbitrary, and Figs. 4–7 use the same range for D_C as is used for the input data ($-0.2 < t < 0.8$ s).

The forms of D_T, D_S, and I are unconstrained, and are not required to determine D_C, although they do affect the physical interpretation of D_C. Rewriting Eq. (9) using Eq. (8) gives

$$D_C(t) = D_T(t) \otimes D_S^{-1}(t), \tag{10}$$

where $D_S^{-1}(t) = \mathcal{F}^{-1}[\tilde{D}_S^{-1}(\omega)]$ is the inverse of the standard task-dependent function. While the functions D_S, D_T, and I can be interpreted physiologically, this is not the case for D_S^{-1}, and hence neither this function nor D_C correspond directly to physiology. However, an approximate physiological interpretation of D_C may be possible, depending on the form of D_S. For example, if D_S is delta-like (e.g., a Gaussian or Mexican hat form centered at $t = 0$), and if the collective activity of the brain is in a linear regime, then D_C can be related to the physiologically meaningful function D_T, since in this case $D_C \approx D_T$ and $I \approx R_S$. However, if D_S has significant temporal structure, or if the brain is in a nonlinear regime, then D_C will not have a direct physiological interpretation, even though it can still be calculated.

2.3. Special cases

In the trivial case where $R_S = R_T$ (i.e., target and standard responses are identical), $\tilde{D}_C(\omega) = 1$, and thus $D_C(t)$ is a delta spike at $t = 0$. This is the simplest possible result, and corresponds to the brain having no task-dependent properties.

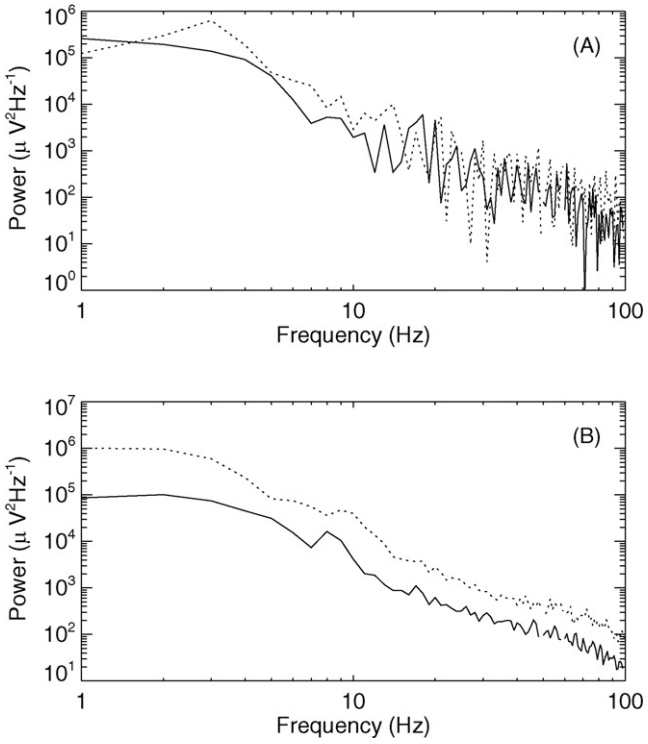

Fig. 3. The spectral power of standard (solid) and target (dotted) EPs. The spectrum above 20 Hz resembles the noise-like power law $P \propto \omega^{-2}$, implying that most of the signal is contained in the frequency band below 20 Hz. (A) Power spectra calculated from the standard and target EPs of a single subject. (B) Power spectra calculated by averaging the spectra of 43 single-subject EPs. The difference in total power between standard and target spectra is largely due to the difference in the number of single trials averaged together to produce each type of EP (280 and 60 for standards and targets, respectively).

As outlined in Section 1, the idealized case closest to experimental EPs is where the target response is a linear superposition of two standards. In this situation, the task-dependent functions D_S and D_T represent impulse functions (e.g., from the thalamus to the cortex); all other properties of the brain remain constant. If D_S is a single delta-like impulse, and if D_T consists of two delta-like impulses separated by a latency difference Δt, then

$$R_S(t) = I(t), \tag{11}$$

$$R_T(t) = \alpha I(t) + \beta I(t - \Delta t), \tag{12}$$

$$R_T(t) = I(t) \otimes [\alpha\delta(t) + \beta\delta(t - \Delta t)], \tag{13}$$

where $\delta(t)$ is a delta function, and α and β are scale factors. Substituting the Fourier transform of Eq. (13) into Eqs. (8) and (9) gives

$$D_C(t) = \mathcal{F}^{-1}\left[\frac{\tilde{D}_T(\omega)}{\tilde{D}_S(\omega)}\right] = \alpha\delta(t) + \beta\delta(t - \Delta t). \tag{14}$$

Thus, if targets are a superposition of two standard responses, we would expect the deconvolution time series D_C to show two delta-like peaks. The areas $A_{0,1}$ of these peaks are equal to the scale factors α and β; the latencies $L_{0,1}$ are determined by the relative latencies of the target and standard. If the N1 components of the target and standard have the same latency, then the first peak will be centered at $L_0 = 0$ ms. The latency of the second peak is primarily determined by the latency difference between target N2 and standard N1, and is thus expected to be $L_1 \approx 100$ ms.

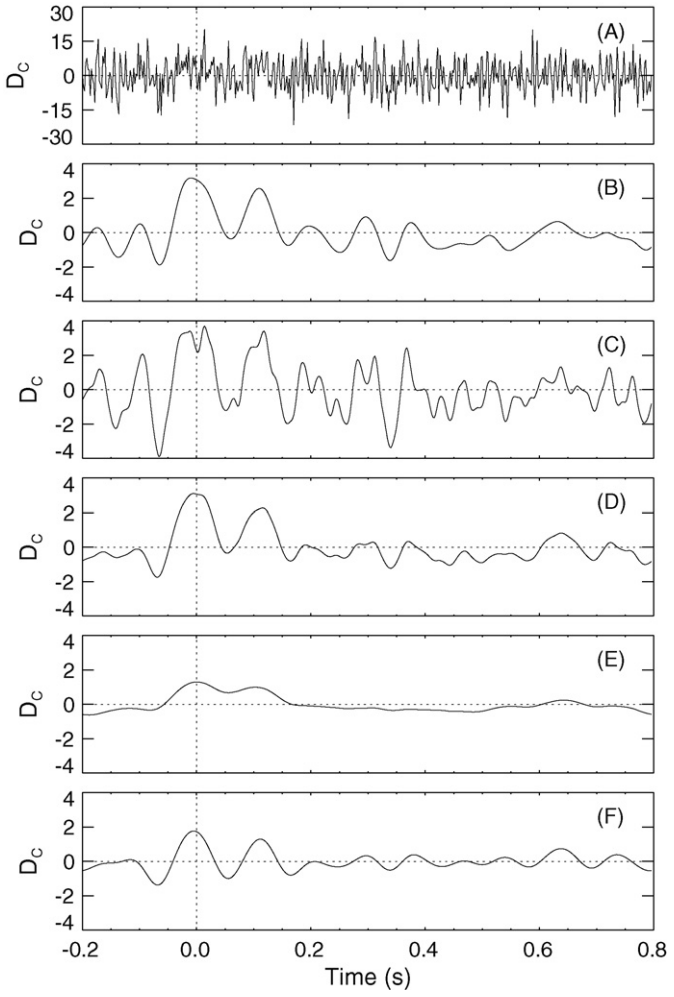

Fig. 4. The effect of different choices of filter on the deconvolution time series, tested using synthetic data. Vertical axes are arbitrary but to scale, showing the large amplitude of the unfiltered deconvolution, and decreasing amplitude with decreasing low-pass cutoff frequency. (A) No filtering. (B) Time-domain smoothing, corresponding to the application of a low-pass filter with a cutoff frequency of approximately 20 Hz. (C) Wiener filtering with a constant NSR, such that the cutoff frequency $f_c \approx 40$ Hz. (D) Wiener filtering with a constant NSR, $f_c \approx 20$ Hz. (E) Wiener filtering with a constant NSR, $f_c \approx 10$ Hz. (F) Wiener filtering using the NSR given by Eq. (18).

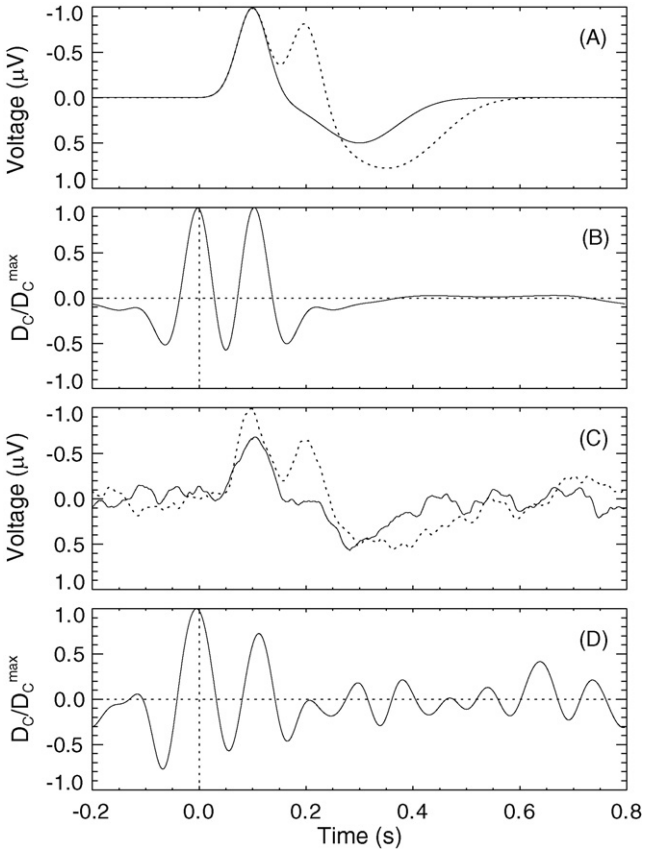

Fig. 5. Deconvolution of synthetic data, showing the effects of low-pass filtering and noise on the deconvolution. (A) Noiseless synthetic standard (solid) and target (dotted) responses. (B) Deconvolution time series D_C for the noiseless synthetic data, showing two clear delta-like spikes, plus oscillatory artifact resulting from low-pass filtering. (C) Synthetic data with noise added such that SNR ≈ 2; standard (solid) and target (dotted) responses are shown. (D) Deconvolution time series D_C for the noisy synthetic data, showing two delta-like peaks, plus artifact and noise.

2.4. Wiener filtering

Since $\tilde{D}_C$ is a ratio of two experimental signals, the deconvolution given by Eq. (7) is highly sensitive to noise. Additionally, since the noise terms in Eq. (7) are divided by $\tilde{R}_S$, small values of $\tilde{R}_S(\omega)$ for a given ω can produce a disproportionate effect on $\tilde{D}_C$. While a large increase in power at a given frequency is unlikely to be due to noise, our data showed apparently random decreases in spectral power at individual frequencies by as much as 10^3, as shown in Fig. 3A. Thus, it is necessary to attenuate frequencies where either $\tilde{N}_S$ or $\tilde{N}_T$ is large, or when $\tilde{R}_S$ is small.

The optimal solution to these problems (in the sense of minimizing mean-squared error) is given by Wiener deconvolution (Wiener, 1949; Walter, 1969; Helstrom, 1967; Jansson, 1984). Provided that an estimate can be made of the power spectra of both the expected signal $\tilde{S}$ and the expected noise $\tilde{N}_T$, Eq. (7) can be replaced with

$$\tilde{D}_C(\omega) = \frac{\tilde{R}_T}{\tilde{R}_S}\left[\frac{|\tilde{R}_S|^2}{|\tilde{R}_S|^2 + \mathrm{NSR}}\right], \tag{15}$$

where the term in brackets is the Wiener filter, and NSR is the noise-to-signal ratio, defined as

$$\mathrm{NSR}(\omega) = \frac{|\tilde{N}_T(\omega)|^2}{|\tilde{S}(\omega)|^2}, \tag{16}$$

where $\tilde{N}_T$ is an estimate of the noise in $\tilde{R}_T$, and $\tilde{S}$ is an estimate of the signal $\tilde{D}_C$. Although the Wiener filter only explicitly incorporates the noise in the target response, there is no reason for $\tilde{N}_S$ and $\tilde{N}_T$ to differ appreciably in spectral content, so the Wiener filter should be equally effective for both sources of noise.

As before, the deconvolution $\tilde{D}_C(\omega)$ given by Eq. (15) can be transformed into a time series $D_C(t)$ using Eq. (9). In the absence of noise, Eq. (15) reduces to Eq. (8). As noise at some frequency increases, the Wiener filter in Eq. (15) attenuates the contribution of that frequency to the overall deconvolution. The most general choices of $\tilde{N}$ and $\tilde{S}$ are white noise (no preferred noise frequencies) and a delta spike in time (all signal times independent), respectively. While this choice produces an acceptable result, we can refine these estimates based on physiological considerations and the experimental EP power spectra.

As shown in Fig. 3, above about 20 Hz, $\tilde{R}_T$ decreases with frequency approximately according to the power law $\tilde{R}_T(\omega) \propto \omega^{-1}$; this type of spectrum is commonly produced by nonstationary noise-like processes (West and Deering, 1994), and is unlikely to contain significant signal. Thus, the noise $\tilde{N}$ is given by the approx-

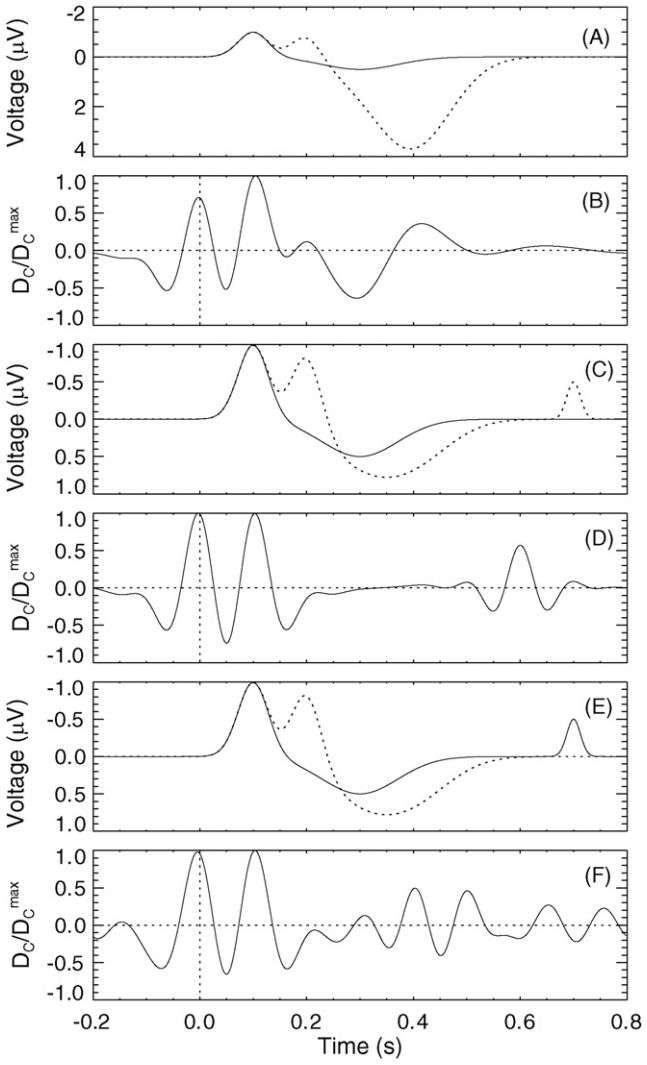

Fig. 6. Deconvolution of synthetic data, showing the effects of perturbations of the EP time series on the deconvolution time series. (A) Synthetic standard (solid) and target (dotted) responses with an augmented target P3, and (B) their deconvolution, showing considerable artifact. (C) Synthetic standard (solid) and target (dotted) responses where an additional feature has added to the target, and (D) their deconvolution, showing only localized effects. (E) Synthetic standard (solid) and target (dotted) responses where an additional feature has been added to the standard, and (F) their deconvolution, demonstrating the sensitivity of deconvolution to noise in the standard.

imation

$$\tilde{N}(\omega) = \alpha\omega^{-1}, \tag{17}$$

where α is a scale factor.

Since the signal $\tilde{S}$ characterizes large-scale processes in the brain, this places an upper bound on its frequency content. Thus, a Gaussian impulse in the time domain describes a signal that is both physiologically plausible and similar to the assumption-free choice of signal $S(t) = \delta(t)$. Combining these estimates of $\tilde{N}$ and $\tilde{S}$ give

$$\mathrm{NSR}(\omega) = \left| \frac{\alpha\omega^{-1}}{e^{-\sigma^2\omega^2}} \right|^2, \tag{18}$$

where the numerator is the noise spectrum $\tilde{N}$ and the denominator is the signal spectrum $\tilde{S}$. The constant α was chosen such that $\mathrm{NSR}(10\,\mathrm{Hz}) \approx 1$, as this is similar to estimates of single-subject NSR, and provided the best empirical result. The constant σ corresponds to the temporal width of the Gaussian signal $S(t)$, and was chosen to be $\sigma = 10$ ms, as this provided optimal filtering of high-frequency noise. The function NSR has minimums at $\omega \approx \pm\sigma^{-1}$, and tends to infinity as $\omega \to 0$ and $\omega \to \pm\infty$. Thus, the Wiener filter defined by Eqs. (15) and (18) has a bandpass character, but any filter with a low-pass cutoff frequency of approximately 15–20 Hz will produce reasonable results. Several different filter choices are demonstrated in Fig. 4, showing that the overall magnitude of NSR (relative to $\tilde{R}_S$) is more important to the deconvolution time series than its precise form (Fig. 4B, D, and F).

2.5. Quantification

If the SNR of the deconvolution time series D_C is high enough that one or more peaks are clearly distinguishable, then D_C can be quantified in terms of their areas and latencies. These peaks are typically much smoother (due to Wiener filtering) and more delta-like than those in the EP time series, and each peak is determined by the entirety of the original time series. Compared to traditional scoring methods, this increases the objectivity and simplicity of quantification, and allows the peaks to be more completely described by only two parameters (latency and area).

Peak latency can be easily and accurately quantified by inspection, since peaks in the deconvolution time series are usually symmetric about their extremums. Additionally, the width of a typical deconvolution feature is approximately half that of a component in the EP time series, allowing greater precision to be obtained.

Peak areas are more difficult to quantify, due to the fact that the signal does not always immediately return to zero on either side of

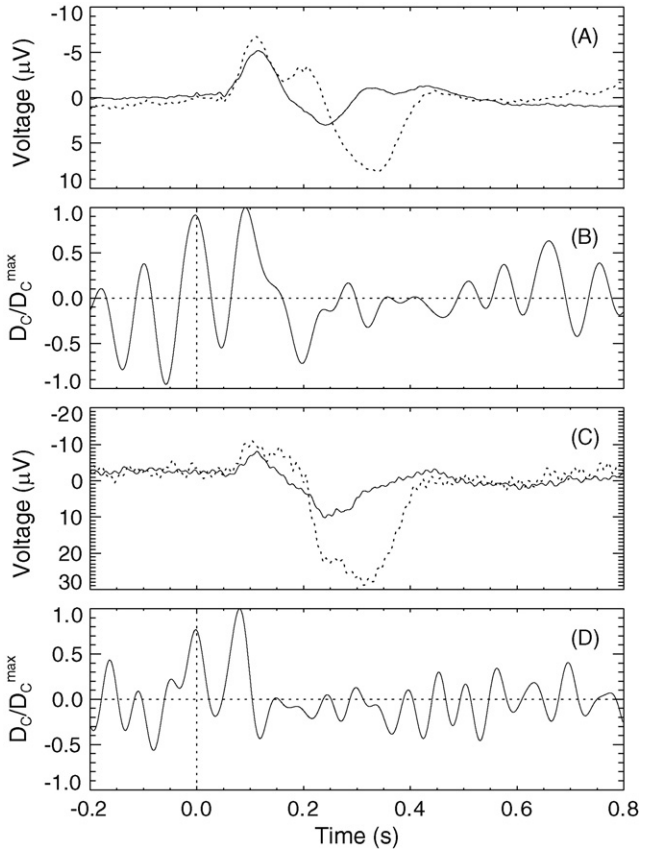

Fig. 7. Deconvolution of experimental EPs. (A) Group average standard (solid) and target (dotted) responses. (B) Deconvolution time series D_C of the group average EPs, showing two clear delta spikes, plus additional signal, oscillatory artifact, and noise. (C) Standard (solid) and target (dotted) responses recorded at the Cz electrode from a single subject. (D) Deconvolution time series D_C for these single-subject EPs, showing two clear delta spikes, despite the absence of a well-defined N2 feature in the target.

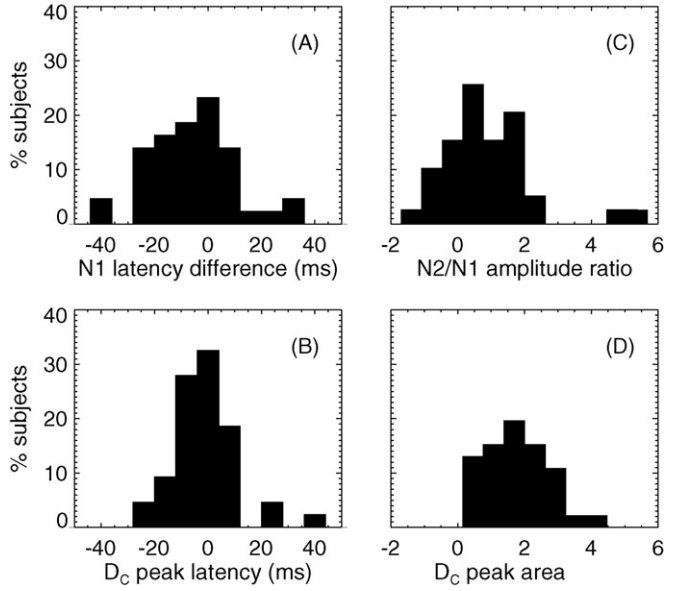

Fig. 8. Distributions of quantitative EP measures for 43 single subjects, comparing measures determined by scoring with equivalent measures in the deconvolution time series. (A) Latency difference between target N1 and standard N1, determined by scoring. (B) Latency of the first peak in the deconvolution time series. (C) Ratio of target N2 amplitude to standard N1 amplitude, determined by scoring. (D) Area of the second peak in the deconvolution time series.

a peak, due to noise or artifact. In cases where it does, peak area A can be calculated by

$$A = C \int_{t_a}^{t_b} D_C(t)\,\mathrm{d}t, \tag{19}$$

where t_a and t_b are the times at which D_C returns to zero on either side of the peak, and C is a normalization coefficient, given by

$$C = \frac{\int_{-\infty}^{\infty} |\tilde{D}'_C \tilde{D}_C|\,\mathrm{d}\omega}{\int_{-\infty}^{\infty} |\tilde{D}_C|^2\,\mathrm{d}\omega}, \tag{20}$$

where $\tilde{D}_C$ is the Wiener-filtered deconvolution spectrum, and $\tilde{D}'_C$ is the spectrum prior to filtering. This normalization coefficient is necessary because the Wiener filter produces attenuation, but not amplification, and hence changes the total power of the deconvolution spectrum. The inclusion of $\tilde{D}_C$ in both the numerator and denominator of Eq. (20) optimizes the normalization factor for the frequencies that contribute most strongly to $\tilde{D}_C$.

3. Results

This section demonstrates the advantages and limitations of the deconvolution method by applying it to the synthetic and experimental data described in Section 2.1. In addition to qualitative comparison with Fig. 2, this section compares quantitative measures of peak amplitude and latency obtained using deconvolution to those obtained using peak scoring.

3.1. Synthetic data

Deconvolution of the noiseless synthetic data produced a time series D_C consisting of two delta-like spikes at latencies $L_0 = 0$ ms and $L_1 = 100$ ms, in exact agreement with prediction, as shown in Fig. 5B. The areas of the two peaks, which measure the amplitudes of the target features with respect to the standard, were $A_0 = A_1 = 1.03$, compared to the ideal value of $A = 1$; relative peak area was identical to the ideal value ($A_1/A_0 = 1$). Wiener filtering causes a truncation of the power spectrum at ~ 20 Hz, and its effect is apparent in Fig. 5B as an oscillatory artifact and a broadening of the spikes. This attenuation of high frequencies is necessary for removing noise in real data, but causes an unavoidable loss of signal; it is compensated for by the normalization coefficient in Eq. (20).

Deconvolution of the noisy synthetic data yielded two delta-like features for 34 out of 40 of trials; an example is shown in Fig. 5D. Despite the fact that peak latencies ($L_0 = 0.2 \pm 3.3$ ms and $L_1 = 103 \pm 4$ ms [mean $\pm$ SEM]) and areas ($A_0 = 0.97 \pm 0.07$, $A_1 = 0.92 \pm 0.08$) both showed considerable variability, their means were very close to the expected values. Hence, even in the presence of significant noise, both qualitative and quantitative results can be obtained using this method. (Note: SEM is used throughout as an approximate indication of uncertainty.)

To investigate the effect of simple perturbations of the input data on the deconvolution, simulation studies were performed by modifying the noiseless synthetic data, as shown in Fig. 6. The addition of a large P3 component to the noiseless synthetic target time series (Fig. 6A) resulted in artifact affecting primarily the region of the time series surrounding the peaks (Fig. 6B; cf. Fig. 5B). The addition of a small-amplitude feature late in the target time series (Fig. 6C) produced only a localized disruption to D_C (Fig. 6D); there was no effect on the two peaks. In contrast, the addition of a small feature in the standard time series (Fig. 6E) created artifact in $D_C(t)$ for all t (Fig. 6F). Thus, although noise in the target time series at time τ will only affect the deconvolution time series at time $t \approx \tau$, noise in the standard will affect the entire deconvolution. The reason can be seen from Eq. (7): a perturbation in R_T corresponds to a nonzero N_T, which has an additive effect on the deconvolution; in contrast, a perturbation in R_S, corresponding to a nonzero N_S, has a multiplicative effect.

3.2. Experimental data

The deconvolution of the group average target EP from the Cz electrode produced two delta-like peaks with a relatively flat baseline, a result qualitatively identical to the noisy synthetic data, as shown in Fig. 7. This supports the hypothesis that target EPs can be largely accounted for as two superimposed standard responses. The negative deflections on either side of the two peaks in Fig. 7B are

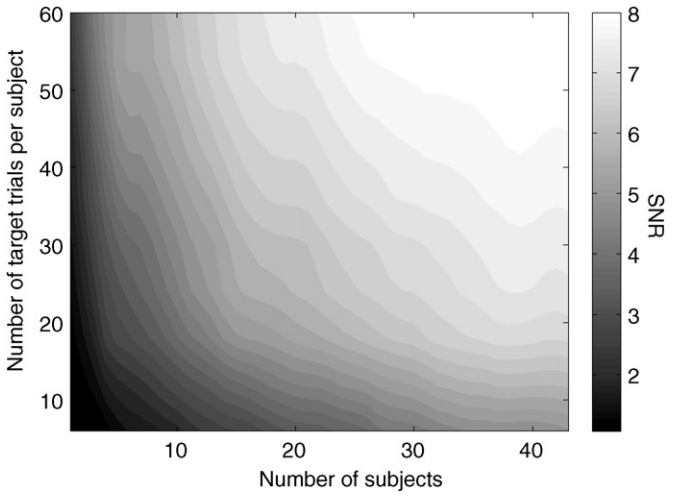

Fig. 9. Effects of the number of subjects (horizontal axis) and number of target trials per subject (vertical axis) used to produce the group average EPs on the SNR of the deconvolution time series (shading). Increasing either the number of subjects or the number of trials per subject increases the SNR of the deconvolution time series, indicating that the SNR is proportional to the total number of trials, regardless of their distribution across subjects.

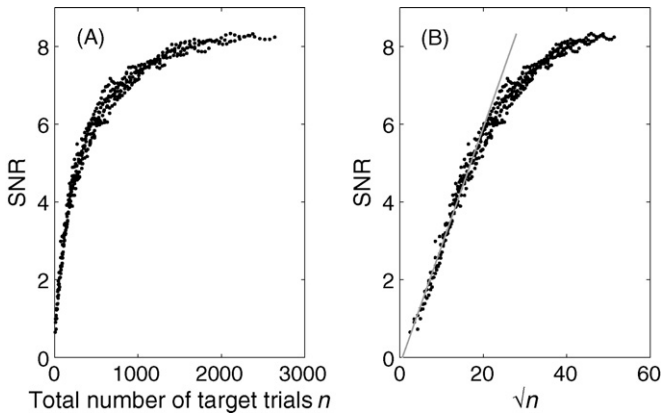

Fig. 10. (A) SNR of the deconvolution time series (vertical axis) as a function of the total number of single target trials (n, horizontal axis). A single subject corresponds to $n = 60$, while the group average corresponds to $n = 2580$. (B) SNR as a function of $\sqrt{n}$, showing a linear relationship for $n < 500$.

partially due to artifact resulting from low-pass filtering, as shown in Fig. 5B.

Of the 43 single-subject target and standard EPs, peak scoring for all EP components (standard N1 and P2; target N1, P2, N2, and P3) was possible for 38 subjects, although these peak scores were unambiguous for only 22 subjects (i.e., only one extremum of the correct sign was present within the given latency range). Deconvolution produced at least one quantifiable peak for 42 subjects; of these, quantification was unambiguous for 31 subjects (i.e., peaks were delta-like, returned to zero on either side, and were of larger amplitude than the rest of the time series). Thus, deconvolution provided unambiguous quantification for nearly 50% more subjects than peak scoring. Significantly, some targets lacking a clear N2 component still produced deconvolutions containing two obvious peaks; an example is shown in Fig. 7C. In contrast to peak scoring, which would suggest an absence of P2 and N2 components, deconvolution analysis implies that both N1 and N2 are still present, but are superimposed into a single broad peak. Deconvolution did not produce useful results for all subjects, however, especially those with either small standard P2 amplitudes or large target P3 amplitudes. This implies that P3 cannot be entirely explained as a superposition of standard P2 features.

3.2.1. Quantification

To evaluate the relative effectiveness of peak scoring and deconvolution as methods of EP quantification, their estimates of component latency and amplitude were compared. To determine the latency difference ΔL_{N1} between target and standard N1 components, the latency score of the standard N1 was subtracted from the latency score of the target N1 for each of the 43 subjects, yielding $\Delta L_{N1} = -5.5 \pm 2.5$ ms (mean ± SEM), as shown in Fig. 8A. The corresponding measurement in the deconvolution time series is the latency of the first peak, which was $L_0 = 0.8 \pm 1.8$ ms. Compared to scoring, this measurement has smaller variance and mean, as shown in Fig. 8B. Furthermore, a Wilcoxon signed-rank test showed that the deconvolution data is consistent with a median latency difference of zero ($p > 0.9$), while scoring data is not ($p < 0.03$). Thus, while both methods show that standard and target N1 latencies are similar, deconvolution allows increased precision for this measurement, and provides stronger evidence that both are generated by the same system. The latency difference between target N2 and standard N1 features determined by peak scoring was $\Delta L_{N2} = 95 \pm 4$ ms, which does not significantly differ from the corresponding value obtained using deconvolution ($L_1 = 96 \pm 3$ ms).

Since the areas A_0 and A_1 of the peaks in the deconvolution time series $D_C(t)$ represent the target/standard amplitude ratios, they can be compared to amplitude ratios determined using peak scoring. The distribution of target/standard N1 amplitude ratios obtained by scoring was 1.8 ± 0.2, which is consistent with the corresponding distribution of deconvolution peak areas ($A_0 = 1.6 \pm 0.1$), according to a Kolmogorov–Smirnov test ($p > 0.5$). In contrast, the target N2/standard N1 amplitude ratio distribution was 1.2 ± 0.2 (Fig. 8C), compared to $A_1 = 2.1 \pm 0.2$ from deconvolution (Fig. 8D), a difference that is highly significant ($p < 0.007$). Although peak scoring yielded larger target N1 amplitudes than N2 amplitudes, this assumes no temporal overlap between target P2 and N2 components. If temporal overlap occurs, it can be removed using deconvolution, allowing a more accurate estimate of N2 amplitude. Since deconvolution yielded peak areas $A_1 > A_0$, this indicates that underlying N2 amplitude may be *larger* than N1 amplitude on average. In summary, for each of the four quantitative results, deconvolution yielded a smaller variance than scoring, reaching statistical significance for the target/standard N1 latency difference (Levene's test, $p < 0.03$) and the target N2/standard N1 amplitude ratio ($p < 0.003$).

3.2.2. Signal-to-noise ratio

To determine the effects of the number of subjects (n_s) and the number of target trials per subject (n_t) on the SNR of the deconvolution time series, an average EP was calculated for each combination of n_s and n_t, up to the limits of the dataset ($n_s = 43$, $n_t = 60$). Deconvolution was performed on the resultant EPs, and the SNR was computed as $\text{SNR} = v_p/v_e - 1$, where v_p and v_e are the variances of the peaks in the deconvolution time series and the region excluding the peaks, respectively. Deconvolution of single-subject EPs gave $\text{SNR} = 2.0 \pm 0.2$, while the group average gave $\text{SNR} = 8.2$, as shown in Fig. 9. The hyperbolic contours in Fig. 9 imply that the SNR is determined by the total number of trials n, regardless of their distribution across subjects; this is also shown by the clustering of points in Fig. 10. For $n < 500$, the SNR of the deconvolution is proportional to $\sqrt{n}$, and hence it can be improved by increasing either the number of subjects or the number of single trials per subject used to generate the EP. Furthermore, the asymptotic behavior above $n \approx 500$ indicates that near-optimal results can be obtained even with a relatively small sample size (8–10 subjects, with 60 target trials per subject).

4. Discussion and summary

This paper presents a method for deconvolving auditory oddball target EPs by using standard EPs, allowing the brain's task-dependent response to be separated from its task-invariant response. In contrast, traditional methods of identifying task-dependent EP features, such as difference signals ("difference waves") and mismatch negativity, require the assumption that the target response consists of task-specific activity superimposed on an unchanged standard response. While such approaches can yield useful results when interpreted carefully, deconvolution allows task-dependent features to be identified without making specific assumptions about the task-invariant response.

Unlike peak scoring, deconvolution allows the separation of temporally superimposed features, as seen in Fig. 7. This shows that targets appearing to lack an N2 component may instead have both N1 and N2 superimposed into a single broad peak, in which case scoring will yield inaccurate amplitudes and latencies for N1 (and omit N2 entirely). Similarly, if there is significant temporal overlap between P2 and N2 components, deconvolution can provide a more accurate estimate of underlying N2 amplitude and latency than is possible using other methods. Additionally, the latency of the first

peak in the deconvolution time series yields a more precise measure of target-standard N1 latency difference than traditional peak scoring.

Both scoring and deconvolution rely on a small number of parameters to quantify the entire EP time series, but deconvolution has two major advantages as a method of target EP quantification. First, whereas peak scores are usually determined by only a handful of points in the data, each peak in the deconvolution time series is determined by the entirety of the original EP time series. Second, due to the delta-like form of the peaks in the deconvolution time series, quantifying these in terms of area and latency allows greater precision and discards less information than the comparable method of scoring EP time series.

Deconvolution produced at least one clear peak for all but one of the single-subject EPs, although many of these deconvolutions also contained significant noise. Since the SNR of the deconvolution time series was found to be directly proportional to the inferred SNR of the input data, it can be improved by increasing the number of single trials used to produce the averaged EPs. This can be achieved by increasing either the number of trials per subject or the number of subjects used to produce the average EPs, with near-optimal SNR provided by approximately 500 target trials, which corresponds to averaging over approximately 10 subjects in a typical paradigm.

The two peaks seen in the deconvolution time series suggest that target EPs (with the exception of P3b) resemble superpositions of two standard EPs, a possibility that can be plausibly explained by thalamocortical loops. The latency difference of approximately 100 ms between the peaks is comparable to the thalamocortical loop delay (e.g., Csépe, 1995; Robinson et al., 2001; Rennie et al., 2002; Rowe et al., 2004; Kerr et al., 2008), implying that, while standards are produced by a single impulse from the thalamus to the cortex, a second thalamocortical impulse is involved in target generation. Additionally, the greater area of the second peak implies transient amplification of the signal, consistent with an excitatory feedback loop. Although this framework may appear to imply that EPs are the result of evoked activity, it is also consistent with EPs being the result of stimulus-induced phase synchronization of ongoing EEG activity, as some authors have recently argued (e.g., Makeig et al., 2002; Martínez-Montes et al., 2008), if the wavelets resulting from phase synchronization can be linearly superposed. In this case, the postulated thalamocortical impulses would result in phase-resetting of ongoing activity in the cortex, as opposed to evoking additional activity.

While it appears that target N1, P2, N2, and P3a features can be accounted for as superpositions of standard N1 and P2 features, the target P3b feature requires a separate explanation. This is consistent with the scalp distributions of these features, since whereas N1, P2, N2, and P3a all have fronto-central scalp distributions, P3b has a parietal distribution, suggesting a distinct generating mechanism (Anderer et al., 1996; Polich, 2003, 2007; Linden, 2005). It may be possible to use deconvolution to separate P3a from P3b, and hence obtain estimates for their amplitudes and latencies, even when they are superimposed as a single P3 feature.

Here we have considered only auditory EPs, as these present the fewest complications, given the comparatively simple anatomy of the auditory cortex. However, this method is applicable to any condition-based paradigm where the resultant time series appear to be partially condition-invariant; hence, deconvolution may be applied to any EP paradigm featuring multiple conditions. Future work will investigate the application of this method to different paradigms, as well as to clinical EP data.

Note: Matlab and IDL implementations of the Wiener deconvolution algorithm described in Section 2 are available for free download from: http://www.physics.usyd.edu.au/complex-systems/.

Acknowledgements

We acknowledge the support of the Brain Resource International Database (under the auspices of Brain Resource; www.brainresource.com) for data acquisition and processing. All scientific decisions are made independently of any Brain Resource commercial decisions via the independently operated scientific division, BRAINnet (www.brainnet.net). We thank the individuals who gave their time to take part in the study. The Australian Research Council supported this work.

References

Alho K. Cerebral generators of mismatch negativity (MMN) and its magnetic counterpart (MMNm) elicited by sound changes. Ear Hear 1995;16:38–51.
Anderer P, Semlitsch H, Saletu B. Multichannel auditory event-related brain potentials: effects of normal aging on the scalp distribution of N1, P2, N2 and P300 latencies and amplitudes. Electroencephalogr Clin Neurophysiol 1996;99:458–72.
Bertero M, Bindi D, Boccacci P, Cattaneo M, Eva C, Lanza V. Application of the projected Landweber method to the estimation of the source time function in seismology. Inverse Prob 1997;13:465–86.
Csépe V. On the origin and development of the mismatch negativity. Ear Hear 1995;16:91–104.
de Weerd J. Facts and fancies about a posteriori "Wiener" filtering. IEEE Trans Biomed Eng 1981;28:252–7.
Delgado R, Özdamar O. Deconvolution of evoked responses obtained at high stimulus rates. J Acoust Soc Am 2004;115:1242–51.
Donchin E, Ritter W, McCallum W. Cognitive psychophysiology: the endogenous components of the ERP. In: Callaway E, Tueting P, Koslow S, editors. Event-related brain potentials in man. New York: Academic Press; 1978. p. 349–411.
Glover G. Deconvolution of impulse response in event-related BOLD fMRI. Neuroimage 1999;9:416–29.
Gordon E, Cooper N, Rennie C, Hermens D, Williams L. Integrative neuroscience: the role of a standardized database. Clin EEG Neurosci 2005;36:64–75.
Gutschalk A, Mase R, Roth R, Ille N, Rupp A, Hähnel S, Picton T, Scherg M. Deconvolution of 40 Hz steady-state fields reveals two overlapping source activities of the human auditory cortex. Clin Neurophysiol 1999;110:856–68.
Haig A, Gordon E, Rogers G, Anderson J. Classification of single-trial ERP sub-types: application of globally optimal vector quantization using simulated annealing. Electroencephalogr Clin Neurophysiol 1995;94:288–97.
Hansen J. Separation of overlapping waveforms having known temporal distributions. J Neurosci Methods 1983;9:127–39.
Helstrom C. Image restoration by the method of least squares. J Opt Soc Am 1967;57:297–303.
Jansson P. Traditional linear deconvolution methods. In: Jansson P, editor. Deconvolution with applications in spectroscopy. Orlando: Academic Press; 1984. p. 67–92.
Jewett D, Caplovitz G, Baird B, Trumpis M, Olson M, Larson-Prior L. The use of QSD (q-sequence deconvolution) to recover superposed, transient evoked-responses. Clin Neurophysiol 2004;115:2754–75.
Kerr C, Rennie C, Robinson P. Physiology-based modeling of cortical auditory evoked potentials. Biol Cybern 2008;98:171–84.
Linden D. The P300: Where in the brain is it produced and what does it tell us? Neuroscientist 2005;11:563–76.
Lines L, Ulrych T. The old and the new in seismic deconvolution and wavelet estimation. Geophys Prospect 2006;25:512–40.
Makeig S, Westerfield M, Jung T, Enghoff S, Townsend J, Courchesne E, Sejnowski T. Dynamic brain sources of visual evoked responses. Science 2002;295:690–4.
Martínez-Montes E, Cuspineda-Bravo E, El-Deredy W, Sánchez-Bornot J, Lage-Castellanos A, Valdés-Sosa P. Exploring event-related brain dynamics with tests on complex valued time-frequency representations. Stat Med 2008;27:2922–47.
Näätänen R. The mismatch negativity: a powerful tool for cognitive neuroscience. Ear Hear 1995;16:16–8.
Nunez P. Removal of reference electrode and volume conduction effects by spatial deconvolution of evoked potentials using a three-concentric sphere model of the head. Electroencephalogr Clin Neurophysiol Suppl 1987;39:143–8.
Özdamar O, Bohórquez J. Signal-to-noise ratio and frequency analysis of continuous loop averaging deconvolution (CLAD) of overlapping evoked potentials. J Acoust Soc Am 2006;119:429–38.
Polich J. Theoretical overview of P3a and P3b. In: Polich J, editor. Detection of change: event-related potential and fMRI findings. Amsterdam: Kluwer Academic; 2003. p. 83–98.
Polich J. Updating P300: An integrative theory of P3a and P3b. Clin Neurophysiol 2007;37:2128–48.
Pritchard W. Psychophysiology of P300. Psychol Bull 1981;89:506–50.
Rennie C, Robinson P, Wright J. Unified neurophysical model of EEG spectra and evoked potentials. Biol Cybern 2002;86:457–71.
Robinson P, Loxley P, O'Connor S, Rennie C. Modal analysis of corticothalamic dynamics, electroencephalographic spectra, and evoked potentials. Phys Rev E 2001;63:041909.

Rowe D, Robinson P, Rennie C. Estimation of neurophysiological parameters from the waking EEG using a biophysical model of brain dynamics. J Theor Biol 2004;231:413–33.
Steriade M, Gloor P, Llinas R, Lopes de Silva F, Mesulam M. Basic mechanisms of cerebral rhythmic activities. Electroencephalogr Clin Neurophysiol 1990;76:481–508.
Ulrych T. Application of homomorphic deconvolution to seismology. Geophysics 1971;36:650–60.
Ungan P, Başar E. Comparison of Wiener filtering and selective averaging of evoked potentials. Electroencephalogr Clin Neurophysiol 1976;40:516–20.
Walter D. A posteriori "Wiener filtering" of average evoked responses. Electroencephalogr Clin Neurophysiol Suppl 1969;27:61–70.
Wang T, Özdamar O, Bohórquez J, Shen Q, Cheour M. Wiener filter deconvolution of overlapping evoked potentials. J Neurosci Methods 2006;15:260–70.
Wastell D. When Wiener filtering is less than optimal: a illustrative application to the brain stem evoked potential. Electroencephalogr Clin Neurophysiol 1981;51:678–82.
West B, Deering W. Fractal physiology for physicists: Levy statistics. Phys Rep 1994;246:6–100.
Wiener N. Extrapolation, interpolation and smoothing of stationary time series with engineering applications. Cambridge, MA: MIT Press; 1949.
Woldorff M. Distortion of ERP averages due to overlap from temporally adjacent ERPs: analysis and correction. Psychophysiology 1993;30:98–119.
Zhang J. Decomposing stimulus and response component waveforms in ERP. J Neurosci Methods 1998;80:49–63.